A Method for Investigating the Orientational Behaviour of Fibrous Particles in Gaseous Flow

Edwin Hirst, Paul H. Kaye, Keith M. Buckley, Spencer J. Saunders*

(Received: 15 July 1994; resubmitted: 13 September 1994)

Abstract

A method is described by which the angular orientation distribution of fibrous particles carried in a gaseous stream may be investigated. The method is based upon the interpretation of the spatial intensity distribution or *scattering profile* of laser light scattered by individual fibres. The scattering instrument used to capture the profiles is described, and the mathematical computation required to ascertain the orientation of each particle at the measurement point is detailed. Illustrative results are given for a study of airborne micromachined silicon particles of 12 μm length and 1.0 μm by 1.5 μm cross-section. The method is currently being employed by the authors to investigate ways of improving the orientation control over nonspherical particles in systems such as aerodynamic particle sizers and particle shape classifiers, since lack of particle orientation control is known to adversely affect the measurement accuracy of both these types of instrument.

1 Introduction

Optical scattering techniques are widely used as a means of counting and sizing airborne particles on an individual basis, and are embodied in a number of commercial instruments. However, in general these instruments do not attempt to assess particle shape but rather attribute a spherical volume equivalent size to each measured particle, based upon an empirical or theoretical calibration function. Particle size spectra may be produced over ranges from sub-micron to tens of microns, though the accuracy and validity of such results has been the subject of some considerable research by workers in the field, for example: *Gebhart* and *Anselm* [1], *Bottlinger* and *Umhauer* [2], and *Killinger* et al. [3]. The problem lies in the fact that the instruments attempt to assess the particle size by measuring the scattered light intensity at one or a range of scattering angles, and that this intensity is usually dependent on not only the particle's size but also its shape and orientation with respect to the incident illumination. (The optical properties of the particle and the wavelength and polarisation state of the radiation are also influencing factors).

Aerodynamic sizing is another commonly used technique for particle characterization, with the TSI *Aerodynamic Particle Sizer* [4], and the Amherst Process Instruments *Aerosizer* [5] perhaps the most popular commercial instruments. Both instruments work on the principle of accelerating an airstream carrying the particles in question, and then measuring the velocities acquired by each particle. Small particles tend to follow the motion of the air whilst larger particles exhibit a lag, thus achieving a lower velocity at the measurement point. The instruments are usually calibrated by observing their behaviour with monodisperse spherical particles. Once again however, errors arise when the instruments are used to measure non-spherical particles since the magnitude of the forces on the particles in the accelerating airflow, and hence the velocities the particles acquire, are critically dependent on the orientation of particles. When investigating the TSI instrument, *Cheng, Chen* and *Yeh* [6] found that the measured aerodynamic diameter of non-spherical particles decreased with increasing shape factor, and similarly *Marshall* et al. [7] found that the true aerodynamic diameters of regular non-spherical particles were underestimated by an average of 25% in the TSI sizer. Whilst correction factors may be employed to reduce these errors with compact non-spherical particles, for more extreme shapes such as fibres, this approach may not be adequate [6]. Identical diameter fibres of different lengths were found to give exactly the same measured size, primarily because variations in the orientations adopted by the different length fibres in the accelerating flow had the effect of counteracting the variations in drag force (and hence particle velocity) which would have otherwise occurred. In both optical particle sizing and aerodynamic sizing therefore, a knowledge of the orientation of non-spherical particles at the point of measurement would allow a significant improvement in the accuracy of measurements. Furthermore, if means could be developed by which greater orientation control could be exerted on the particles so as to render non-spherical uniformly oriented whilst under measurement, the task of extracting valid size and indeed shape data would be considerably eased.

For several years, the authors have been engaged in the development of instruments and techniques aimed at the classification of airborne particles on the basis of both size and shape. The techniques have been based on the interpretation of the spatial light scattering properties of individual particles in flow as a means of establishing shape and size indices for the particles (*Kaye* et al. [8-11]). As part of the investigations, we required a method for accurately determining the orientation behaviour of highly non-spherical particles in airflow delivery systems. This was to facilitate current investigations into the optimisation of the aerodynamics of the delivery systems and into the

* Dr. *E. Hirst*, Prof. *P. H. Kaye, K. M. Buckley, S. J. Saunders*, Engineering Research and Development Centre, University of Hertfordshire, Hatfield, Hertfordshire AL10 9AB (United Kingdom).

 0934-0866/95/0102-0003 $5.00 + .25/0

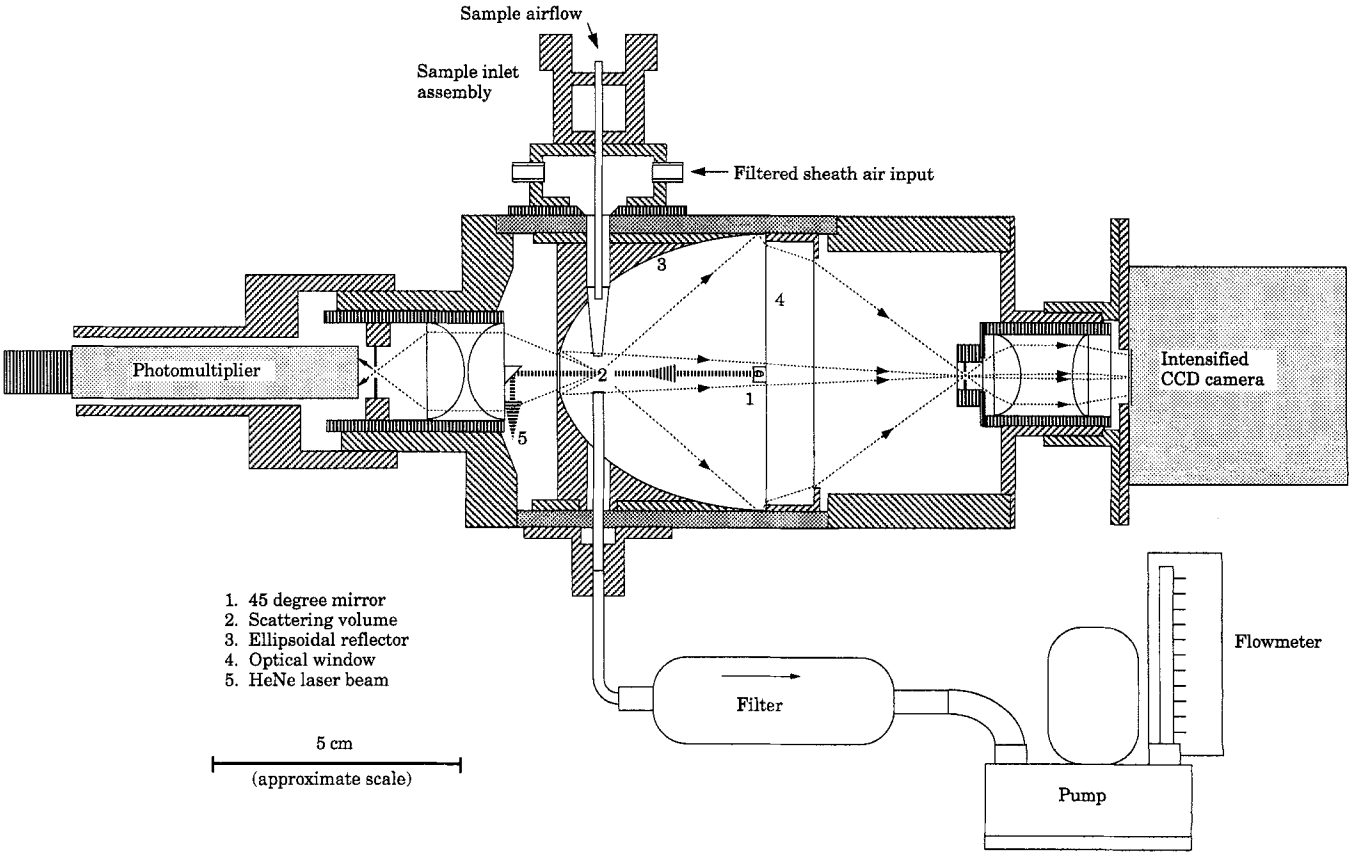

Fig. 1: Schematic diagram of the laser scattering chamber used in the study of particle orientation behaviour. The beam from a diode laser (not shown) enters the chamber orthogonal to the paper and is redirected along the optical axis by a 45° mirror so as to intercept the sample airflow carrying the particles at the focus of the ellipsoidal reflector.

possible use of other phenomena, such as electrostatic alignment, as a means of achieving maximum control over particle orientation. This paper describes the method by which the orientation behaviour of non-spherical particles carried in a moving airstream may be accurately determined.

2 Apparatus

The light scattering system being used in the investigations is shown schematically in Figure 1, and is described in detail elsewhere [10]. The radiation source (not shown) is a linearly polarised 9 mW diode laser operating at 670 nm wavelength arranged with the beam axis perpendicular to the paper in Figure 1. Radiation from the laser is directed through a collimator, iris diaphragm, and cylindrical lens into the scattering chamber where it strikes a 45° front silvered mirror (labelled 1) with the plane of polarisation of the beam being perpendicular to the plane of incidence at the mirror. The radiation is focused to an approximately ellipsoidal cross-section (3 mm width by 100 μm depth) at a point within the scattering chamber coincident with the transverse flow of incoming sample air. The unscattered beam then passes on to a second 45° mirror and is subsequently absorbed within a baffle chamber.

Particle laden air is drawn into the scattering chamber through the interchangeable inlet nozzle and intersects the laser beam, thus defining the *scattering volume* of approximately 1 mm diameter (determined by a sample column cross-section) and 100 μm depth (determined by the beam depth). Particle trajectories may occur anywhere through the scattering volume cross-section, and this uncertainty in position has some effect on the accuracy of particle orientation measurements (see Section 4.1). The internal design and position of the inlet nozzle relative to the laser beam, the airflow velocity and degree of sheath flow used to produce aerodynamic focusing, are all factors which are subject to variation in the current investigations of particle orientation optimisation.

Individual particles in the sample air traverse the laser beam and produce pulses of scattered light of ~3 μs duration. Light scattered into angles between 28° and 141° to the beam direction and around the full 360° of azimuth is incident upon an ellipsoidal reflector whose primary focus is coincident with the scattering volume. The reflected light is refocused onto the photocathode of an intensified CCD (charge-coupled device) camera. The camera output image is therefore a two-dimensional transform of the transient three-dimensional spatial intensity distribution falling onto the ellipsoidal reflector, and corresponds to approximately 83% of the total sphere of scattering about the particle. This image is termed the *scattering profile*. Light scattered from the particle into angles between 5° and 27° is focused onto a photomultiplier detector, the output signal from which is used to trigger image acquisition on the CCD camera.

3 Experimental Procedure

The investigation of the relationship between particle shape and orientation within specified flow configurations, and moreover the investigations into how those flow configurations might be modified to improve orientation control, required the use of highly monodisperse particle populations to ensure that statisti-

cally valid data could be obtained. For this purpose we used the process of silicon micromachining to manufacture the necessary particle types. Silicon micromachining is a technology derived from the electronic microchip industry which offers unparalleled uniformity and reproducibility for non-spherical particle geometries. The processing employed by the authors is described in detail elsewhere (*Kaye* et al. [12]), and the resulting particle types, manufactured in both silicon and silicon dioxide, exhibited a standard cross-section of 1.0 μm by 1.5 μm, and lengths of 3 μm, 5 μm, 8 μm, 12 μm, 18 μm, and 25 μm (each length ± 0.2 μm). Figure 2 shows an electron micrograph of a sample of the fibrous particles – silicon dioxide fibres of 12 μm length – which were used in the preliminary results given later in this paper.

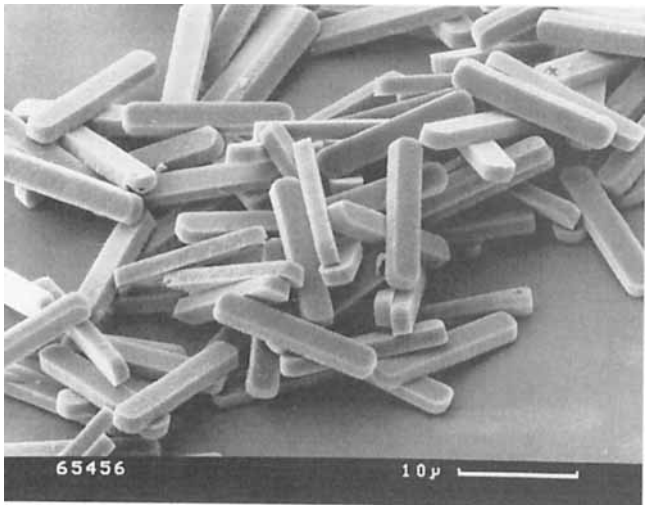

Fig. 2: Scanning electron micrograph of highly monodisperse silicon dioxide fibres used within the study of particle orientation behaviour. The particles were of 12 μm length and 1.0 μm by 1.5 μm cross-section and were produced using the process of silicon micromachining. Other particle types from 3 μm to 25 μm length and similar cross-section were also produced.

3.1 Light Scattering Data

Figure 3 shows a typical scattering profile image recorded from a single 12 μm long silicon dioxide fibre. The image was recorded over a 3 μs exposure as the fibre passed through the scattering volume with a velocity in this case of 33 (±2) ms^{-1} (derived from the total transit time through the beam). It represents essentially a scattered photon distribution map, the result of several thousand photons scattered by the particle to the faceplate of the image intensifier. The innermost dark circle at the centre of the image corresponds to scattering at 28° to the laser beam propagation axis, this axis being perpendicular to the plane of the paper. The outer circumference corresponds to scattering at 141° to the beam axis. These angular limits are defined by the inner and outer edges of the ellipsoidal mirror within the scattering chamber. The vertical dumb-bell shaped shadow is an artefact of the instrument, being caused by the sample airflow inlet and exit tubes; the centres of the two circular shadows thus represent 90° scattering directly above and below the particle.

The example given in Figure 3 is of a fibre aligned vertically, i.e.: parallel to the axis of the airflow and perpendicular to the incident laser beam. This particle orientation results in the observed horizontal scattering bars, and the angular positions of the intensity minima discernible in the scattering bars may be

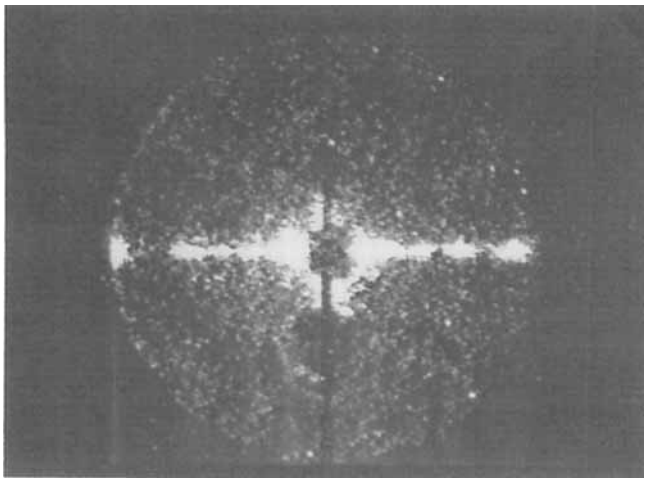

Fig. 3: Scattering profile image recorded from a single 12 μm long silicon dioxide fibre within the sample airflow. The image was recorded in a period of 3 μs, with each white dot representing a single scattered photon. The inner boundary corresponds to scattering at 28° and the outer circumference to scattering at 141° to the axis of the illuminating laser beam. The horizontal scattering bars indicate that the particle was vertical (i.e.: parallel to the axis of the airflow) at the point of measurement.

related to a first order to the cross-sectional dimensions of the fibre. With fibres which are misaligned from vertical, the scattering assumes conic section form as predicted by theory [13] and as illustrated in the profiles shown in Figure 4. These profiles, each recorded from essentially identical particles, highlight the effects (clockwise from top-left) of increasing particle misalignment, the extreme case being when the complete cone of scattered light is intercepted by the reflector and the scattering profile assumes a circular form. The cone of scattered light is coaxial with the fibre axis and tangential to the direction of the incident beam, with the centre of the fibre at the apex of the cone. The example shown in the bottom-left of Figure 4 corresponds to a fibre misaligned by 18° from the vertical, i.e. the upper tip of the fibre is tilted backwards from the incident laser beam direction. In this example the fibre has an azimuth

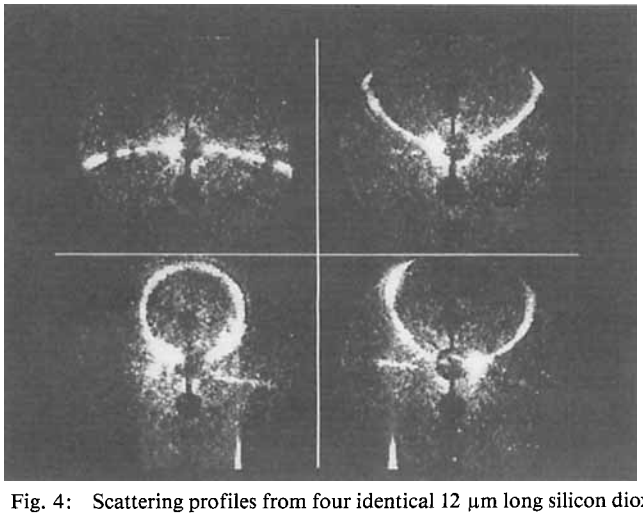

Fig. 4: Scattering profiles from four identical 12 μm long silicon dioxide fibres with (clockwise from top-left) increasing misalignment from the axis of the airflow. Each scattering profile is a conic section, becoming a complete circle in the most highly misaligned case (here the particle is misaligned 18° from the axis of the airflow).

angle ϕ of approximately $-5°$, with the angle defined anticlockwise from the vertical. It is from numerous images of this type that the alignment behaviour of the fibres within the flow may be determined using the method described below.

4 Data Analysis Method

Determination of alignment angle of each fibre is carried out from its corresponding profile using one of two computerised measurement methods, depending on whether or not the complete cone of scattering is intercepted by the ellipsoidal reflector. For profiles where the scattering bars intercept the outer circumference of the profile, the azimuth angle ϕ is determined from the angles θ_1 and θ_2 shown in Figure 5(a). These angles are measured using dedicated image processing software and

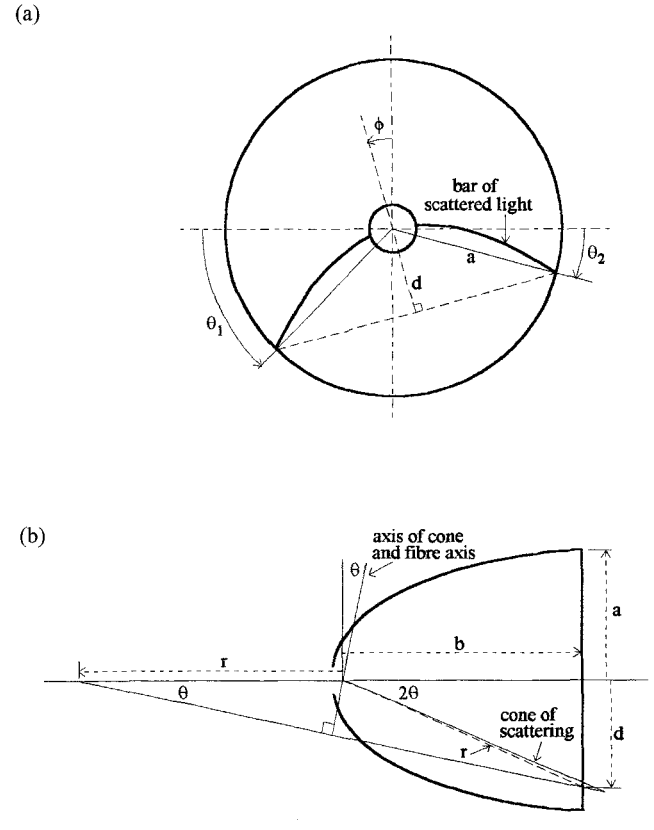

Fig. 5: (a) Schematic diagram of a profile from a fibre where the cone of light is not completely captured, showing the dimensions as defined in the text and the derivation of angles θ_1 and θ_2. (b) Cross-section through the optical axis of the reflector and the cone of scattering. The line labelled r in long dashes is not in the plane of the paper, but lies along the scattered cone between the fibre and the edge of the reflector. Hence both r and b are almost constant, only varying with particle lateral position within the scattering volume.

recorded in a computer database. The error in assessment of these angles has been estimated at $\pm 1.5°$. For profiles where the complete cone of scattering is intercepted to produce a circular conic section, the fibre azimuth angle is determined directly as the angle ϕ between the vertical axis and the bisector of the conic section, again with an estimated measurement error of $\pm 1.5°$. The scattering angle corresponding to the outermost edge of the conic section is also determined from a knowledge of the geometric mapping of the scattering angles (between 28° and 141°) onto the profile images. The error in this measurement depends on the scattering angle and is derived in the following section. Again, the two angles are recorded in a computer database.

4.1 Alignment Angle Derivation

4.1.1 Incomplete Scattering Cone Interception

Figure 5(a) shows schematically a profile for cases where the complete cone of scattering is not intercepted by the reflector. Geometrically, profiles are the projection of the locus of intersection of the scattering cone with the ellipsoidal reflector on the plane containing the edge of the reflector, hence this plane is parallel to the yz plane in Figure 6. Figure 5(b) shows a cross-

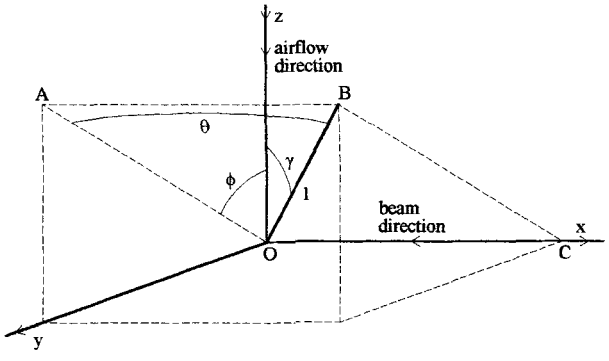

Fig. 6: Diagram showing the relationship between the fibre alignment angle γ relative to the airflow and azimuth and polar scattering angles ϕ and θ for a fibre of length 1. ϕ is defined in the yz plane and θ in the plane ABCO.

section of the scattering chamber through the optical axis and the axis of revolution of the cone of scattered light. This plane also contains the fibre axis, with the apex of the cone coinciding with the centre of the fibre, and is the plane ABCO in Figure 6. The azimuth angle ϕ measured relative to the vertical is, from Figure 5(a),

$$\phi = \pi/2 - \theta_2 - (\pi - \theta_1 - \theta_2)/2 = (\theta_1 - \theta_2)/2 \,. \quad (1)$$

The polar angle θ is, from Figure 5(b),

$$\tan\theta = d/(r + b)$$

where d is the perpendicular distance from the centre of the profile to a line drawn between the ends of the arc as shown in Figure 5(a), b is the perpendicular distance from the apex of the cone to the plane containing the edge of the reflector and r is the distance between the apex and the edge of the reflector. r is given by $\sqrt{a^2 + b^2}$, where a is the radius of the ellipsoidal reflector. From Figure 5(a), the distance d is given by

$$d = a|\cos((\pi - \theta_1 - \theta_2)/2)| = a|\sin((\theta_1 + \theta_2)/2)|$$

giving

$$\tan\theta = a|\sin((\theta_1 + \theta_2)/2)|/(\sqrt{a^2 + b^2} + b) \,. \quad (2)$$

From Figure 6, the projection of the fibre on to a plane perpendicular to the airflow is given by the equations

$$x = l\sin\theta \text{ and } y = l\cos\theta\sin\phi$$

where l is the length of the fibre. The airflow alignment angle γ is then given by

$$\sin\gamma = \sqrt{x^2 + y^2}/1 = \sqrt{\sin^2\theta + \cos^2\theta \sin^2\phi} \ . \quad (3)$$

The error in estimating ϕ is given by

$$\Delta\phi = \frac{\partial\phi}{\partial\theta_1}\Delta\theta_1 + \frac{\partial\phi}{\partial\theta_2}\Delta\theta_2 = (\Delta\theta_1 \pm \Delta\theta_2)/2$$

since from Eq. (1) both partial derivatives are 0.5. Since the uncertainty in both θ_1 and θ_2 is $\pm 1.5°$, the worst case error in ϕ is $\pm 1.5°$. The worst case error has been deliberately chosen over the root mean square error to encompass all possible error situations.
The error in estimating θ is given by

$$\Delta\theta = \frac{\partial\theta}{\partial\theta_1}\Delta\theta_1 + \frac{\partial\theta}{\partial\theta_2}\Delta\theta_2 + \frac{\partial\theta}{\partial b}\Delta b \ .$$

The dependence on b is due to the fact that the fibre may pass at any point through the scattering volume defined by the intersection of the airflow and the laser beam. The partial derivative with respect to θ_1 or θ_2 is, from Eq. (2),

$$\frac{\partial\theta}{\partial\theta_1}\sec^2\theta = \frac{k}{2}\cos((\theta_1 + \theta_2)/2)$$

where

$$k = a/(\sqrt{a^2 + b^2} + b) \ .$$

This gives

$$\frac{\partial\theta}{\partial\theta_1} = \frac{\partial\theta}{\partial\theta_2} = \frac{k\cos((\theta_1 + \theta_2)/2)}{2(1 + k^2\sin^2((\theta_1 + \theta_2)/2))} \ .$$

The worst case value occurs when $\theta_1 + \theta_2$ is zero. For a particle at the focus, the values of a and b are respectively 37.2 mm and 46.73 mm, which are derived from the quoted reflector dimensions. k then has a value of 0.175 rad/rad and the worst case error due to θ_1 and θ_2 is 0.524° for an uncertainty in $\Delta\theta_1$ and $\Delta\theta_2$ of $\pm 1.5°$. The partial derivative with respect to b is, from Eq. (2),

$$\frac{\partial\theta}{\partial b}\sec^2\theta = \frac{-k(b(a^2 + b^2)^{-1/2} + 1)}{((a^2 + b^2)^{1/2} + b)^2}$$

where

$$k = a|\sin((\theta_1 + \theta_2)/2)| \ .$$

This gives

$$\frac{\partial\theta}{\partial b} = \frac{-k(b(a^2 + b^2)^{-1/2} + 1)}{k^2 + ((a^2 + b^2)^{1/2} + b)^2} \ .$$

Since this is a monotonically increasing function with k, the worst case value occurs when k is equal to a. The derivative, which is insensitive to small changes in b, then has a value of 5.2×10^{-3} rad/mm. The maximum value for Δb is 0.5 mm giving a worst case error due to particle position of 2.6×10^{-3} rad or 0.15°. This occurs when $\theta_1 + \theta_2$ equals π, which means that the worst case errors are not additive since they occur at opposite extremes of the polar angles measured by this method.

The total error is given by

$$\Delta\gamma = \frac{\partial\gamma}{\partial\theta}\Delta\theta + \frac{\partial\gamma}{\partial\phi}\Delta\phi \ .$$

From Eq. (3), the partial derivative with respect to θ is

$$\frac{\partial\gamma}{\partial\theta}\cos\gamma = \frac{\sin\theta\cos\theta - \sin\theta\cos\theta\sin^2\phi}{(\sin^2\theta + \cos^2\theta\sin^2\phi)^{1/2}}$$

which simplifies to

$$\frac{\partial\gamma}{\partial\theta} = \frac{\sin\theta\cos\phi}{(\sin^2\theta + \cos^2\theta\sin^2\phi)^{1/2}} \ .$$

The partial derivative with respect to ϕ is similar and is given by

$$\frac{\partial\gamma}{\partial\phi} = \frac{\cos\theta\sin\phi}{(\sin^2\theta + \cos^2\theta\sin^2\phi)^{1/2}} \ .$$

These equations are included in the computation of the alignment angle and error estimate for each profile analysed.

4.1.2 Complete Scattering Cone Interception

For cases where the complete cone is intercepted by the reflector, the azimuth angle ϕ can be measured directly from the scattering profile as detailed previously and shown in Figure 7(a). The estimated error in this measurement is $\pm 1.5°$. The polar angle θ is derived from a measurement of the scattering position on the profile for the outermost point of the circular scattering ring as shown in Figure 7(a). The scattering angle corresponding to this point is determined from a knowledge of the mapping of the scattering angles between 28° and 141° onto the scattering profile format. From Figure 7(b), the polar fibre angle θ is then given by

$$\theta = (\pi - \theta_s)/2 \ .$$

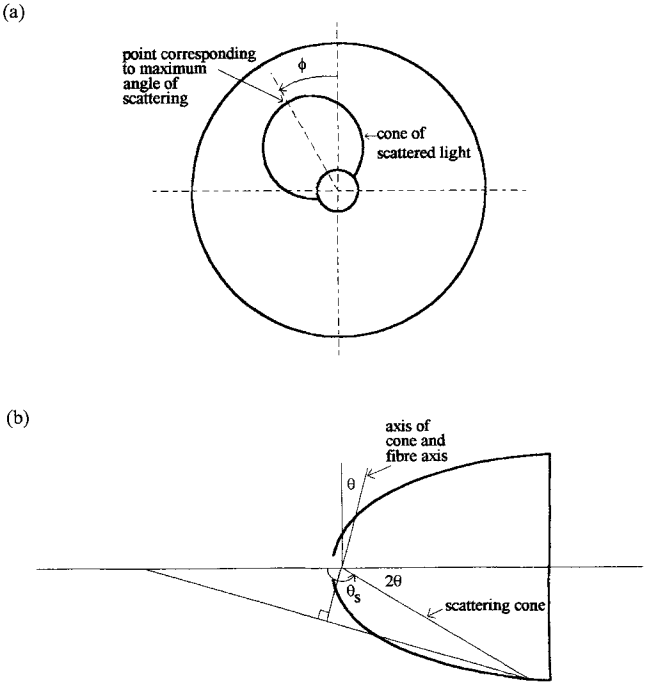

Fig. 7: (a) Schematic diagram of a profile from a fibre where the cone of light is completely captured, showing the direct measurement of ϕ. (b) Cross-section through the optical axis of the reflector and the cone of scattering.

The alignment angle is then given by Eq. (3) as before.
The error involved in measuring the angle 2θ was determined empirically by measuring the apparent change in the scattering angles on the profiles for particles at the extremes of the scattering volume. The apparent changes were then graphed and a worst case line drawn. The equation of the line was calculated as

$$\Delta(2\theta) = 8.58 - 0.056(2\theta) .$$

The error for θ is half this value. The total error for the alignment angle was then calculated as before. Again, these equations are included in the computation of the alignment angle and error estimate for each profile analysed.

5 Preliminary Results

As an illustration of the procedure described above, a preliminary experiment is described in which the alignment behaviour of the 12 μm silicon dioxide fibres mentioned in Section 3 was addressed. An aerosol of the fibres was produced in a large containment vessel using a TSI Tri-Jet Aerosol Generator (TSI Inc. St. Paul, MN, USA). In the first part of the experiment, fibres were delivered into the scattering chamber in an airflow drawn from the containment vessel at a volume flowrate of 1.5 l/min., together with a filtered sheath-flow of 3.5 l/min. This produced a flow Reynolds Number of 2000 (sub-turbulent). The exact details of the geometry of the delivery system and flow conditions are not given here but will form part of a more thorough reported study within a future communication. In the second part of the experiment fibres of identical form were delivered under the same flow conditions except for the additional presence of an electric field set up between the inlet and outlet airflow tubes by applying a -2 kV potential to the outlet tube (the inlet tube being grounded). This gave an average electric field strength of 2 V/μm between the tube tips and was intended to provide a first cursory assessment of the effect such fields may have on particle alignment. The fibres were known to carry a residual charge produced during the aerosol generation process.
The alignment angle distribution for the fibres both with and without the electric field is shown in histogram form in Figure 8. The statistical analysis of the results is given in Table 1. The results in both cases have a Poisson distribution as might be expected, with a mean particle alignment angle of 23.2° with no electric field present and of 21.3° in the presence of the field, with the mean measurement errors for the two cases were ±1.37° and ±1.36° respectively. This indicated that assuming the central limit theorem holds, the improvement in alignment with the electric field, though modest, was nevertheless statistically significant.

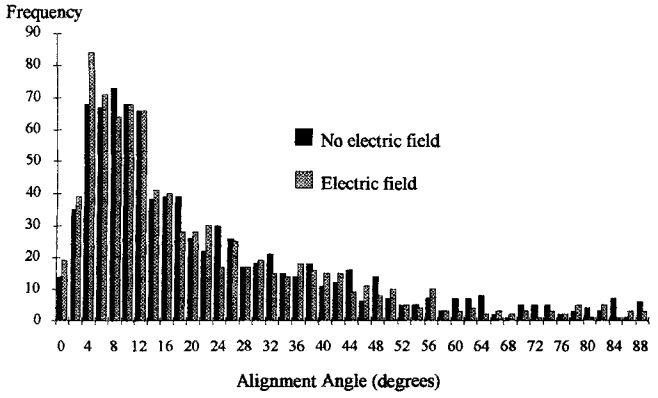

Fig. 8: Histogram showing the alignment angle distribution of 12 μm long silicon dioxide fibres delivered from an aerodynamic focusing nozzle both with and without an electric field of 2 V/μm applied between the nozzle and the outlet tube (see Figure 1). The field in this case produces a modest improvement in the mean alignment angle, reducing it from 23.2° to 21.3°.

Table 1: Statistical data for the alignment angle distribution experiment carried out with 12 μm silicon dioxide fibres both with and without a 2 V/μm electric field between the airflow inlet nozzle and the outlet tube.

	No electric field	Electric field applied
Number of fibres measured	866	850
Mean alignment angle	23.2°	21.3°
Median alignment angle	16.0°	14.5°
Sample standard deviation	19.84°	18.42°
Mean measurement error	±1.37°	±1.36°
% within 20° alignment	59	61
% within 30° alignment	73	75

6 Discussion

The experiment outlined above is intended principally to illustrate the accuracy with which the alignment behaviour of airborne particles may be investigated using the light scattering method described. The ability to ascertain the orientation of non-spherical particles with respect to the airflow supporting them, and to analyse statistically significant numbers of particles within a reasonable time period, will aid fundamental studies into the behaviour of such particles under various flow conditions. The authors are currently engaged in the development of airflow delivery nozzles with a view to optimising particle orientation control by both aerodynamic means and, where appropriate, electrostatic means. This work will form the basis of a future communication. It is anticipated that the results of this work may be of value in improving the accuracy of optical and aerodynamic particle sizing instruments by allowing better characterization and calibration for non-spherical particles.

7 Acknowledgement

The authors wish to thank the UK Engineering and Physical Sciences Research Council and the UK Ministry of Defence for their support of this work.

8 Symbols and Abbreviations

a	radius of the reflector
b	perpendicular distance from the fibre to the plane containing the edge of the reflector
d	perpendicular distance from the optical axis of the instrument to the line between the ends of the scattered arc of light in the plane containing the edge of the reflector
r	distance from the fibre to the edge of the reflector
l	fibre length

x and y coordinates in the plane orthogonal to the airflow, x being the opposite direction to the laser beam direction

γ angle between the airflow direction and the long axis of the fibre in the plane containing the axis and the airflow

θ angle between the normal to the beam direction and the long axis of the fibre in the plane containing the axis and the laser beam

θ_1 and θ_2 angles between the horizontal and the bars of scattered light on fibre profiles as shown in Figure 5(a)

θ_s scattering angle in relation to the laser beam direction

ϕ angle between the vertical (airflow direction) and the long axis of the fibre in the plane of the profiles

9 References

[1] *J. Gebhart, A. Anshelm:* Effect of Particle Shape on the Response of Single Particle Optical Counters. Proc. Int. Symp. Optical Particle Sizing, Theory and Practice. Plenum, 1988, pp. 393–409.

[2] *M. Bottlinger, H. Umhauer:* Scattered Light Particle-size Counting Analysis – Influence of Shape and Structure. Proc. Int. Symp. Optical Particle Sizing, Theory and Practice. Plenum, 1988, pp. 363–369.

[3] *R. T. Killinger, R. H. Zerull:* Effects of Shape and Orientation to be considered for Optical Particle Sizing. Proc. Int. Symp. Optical Particle Sizing, Theory and Practice. Plenum, 1988, pp. 419–429.

[4] Aerodynamic Particle Sizer APS 3310; manufactured by TSI Inc., St. Paul, MN, USA.

[5] Aerosizer; manufactured by Amherst Process Instruments Inc., MA, USA.

[6] *Y. S. Cheng, B. T. Chen, H. C. Yeh:* Behaviour of Isometric Non-spherical Aerosol Particles in the Aerodynamic Particle Sizer. J. Aerosol Sci. *21* (1990) 701–710.

[7] *I. A. Marshall, J. P. Mitchell, W. D. Griffiths:* The Behaviour of Regular Shaped Non-spherical Particles in a TSI Aerodynamic Particle Sizer. J. Aerosol Sci. *22* (1991) 73–89.

[8] *P. H. Kaye, N. A. Eyles, J. M. Clark:* A Laser Scattering Instrument for Airborne Particle Size and Shape Classification. Proc. 2nd Int. Congr. on Optical Particle Sizing. Univ. of Arizona, Phoenix, USA, 1990, pp. 501–510.

[9] *P. H. Kaye, N. A. Eyles, I. K. Ludlow, J. M. Clark:* An Instrument for the Classification of Airborne Particles on the Basis of Size, Shape and Count Frequency. Atmos. Environ. *25A* (1991) 645–654.

[10] *P. H. Kaye, E. Hirst, J. M. Clark, F. Micheli:* Airborne Particle Shape and Size Classification from Spatial Light Scattering Profiles. J. Aerosol Sci. *23* S1 (1992) 597–611.

[11] *P. H. Kaye, E. Hirst, F. Micheli:* The Characterisation of Airborne Particles by Analysis of Spatial Light Scattering Profiles. J. Aerosol Sci. *23* S1 (1992) 321–324.

[12] *P. H. Kaye, F. Micheli, M. C. Tracey, E. Hirst, A. M. Gundlach:* The Production of Precision Silicon Micromachined Non-spherical Particles for Aerosol Studies. J. Aerosol Sci. *23* (1992) 201–204.

[13] *C. F. Bohren, D. R. Huffman:* Absorption and Scattering of Light by Small Particles. Wiley, New York 1983, pp. 201–210.